Diagnosing El Niño - La Niña Transitions

Matthew S. Spydell

1 Introduction

Climate variability on interannual time scales is exemplified by the El Niño -Southern Oscillation (ENSO). An El Niño event is marked by anomalously warm SST's in the eastern portion of the equatorial Pacific and the weakening of the trade winds over much of the equatorial Pacific, the opposite event is called La Niña. In addition to locally affecting the climate near the equator, El Niño and La Niña significantly affect the weather throughout the Americas. A standard ENSO index is the anomalous surface atmospheric pressure difference between Tahiti and Darwin, Australia. As a time series, this index shows significant variability around the $1/4$ yr^{-1} frequency. Although much research has been devoted to the study of ENSO, there are still some open issues regarding: what starts El Niño, what sustains its quasi-periodic behavior, etc. Two complementary conceptual models of ENSO have been successful in exposing some of the main dynamics of ENSO.

Prior to the development of these conceptual models an intermediate model of ENSO was developed by Zebiac and Cane [1]. This model (henceforth ZCM) is a coupled ocean-atmosphere model that uses a steady state linearized atmosphere, and long-wave linear momentum equations for the ocean. The atmospheric model is essentially a Gill type equatorial model [2]. The ocean and atmosphere are coupled through the atmosphere being forced by anomalous SST's, and the ocean being forced by anomalous wind stresses. This model was shown to have variability similar to ENSO. However, it was difficult to show exactly what mechanisms resulted in ENSO variability because of the model's complexity.

In an effort to understand the basic mechanisms that result in ENSO variability, Battisti (1988) and Schopf & Suarez (1988) showed that the ZCM can be reduced to a delayed oscillator model that contains ENSO-like variability ([3] and [4]). The delayed oscillator model of ENSO emphasizes the role of equatorially trapped waves and the different crossing times of Kelvin and Rossby waves as the source of ENSO-like variability. Specifically, by integrating along characteristics of Kelvin and Rossby waves, and after making some simplifying assumptions, the delayed oscillator equation, $dT/dt = aT - bT(t-\tau) + \mathcal{N}$, was derived. The aT term represents the positive El Niño feedback and the $-bT(t-\tau)$ term represents the delay effect of the Rossby waves which effectively carry temperature of the opposite sign to the eastern equatorial region at a time τ later. It is this delay that is crucial to ENSO variability.

In 1997 a different conceptual model of ENSO was developed by Jin ([5] and [6]). This model is a recharge oscillator model and it deemphasizes the role of waves as the mechanism

of variability and emphasizes the role of mass transport as the mechanism responsible for ENSO variability. Specifically, this model shows that it is the different adjustment times that is responsible for ENSO variability: the thermocline slope adjusts almost instantly to wind stress changes, and the mass (volume) of the equatorial strip takes more time to adjust to wind stress changes. In this model it is crucial for the equatorial strips volume to oscillate in time; anomalous mass must be transported into the equatorial strip in order for an El Niño event to occur.

The purpose of this work is to see if the conceptual models are in agreement with idealize El Niño to La Niña transitions as produced by a shallow water model forced by periodic El Niño - La Niña wind stresses. Specifically, the following questions were addressed. One, are the delayed oscillator and the recharge oscillator complementary views of ENSO variability? Two, from the recharge oscillator perspective what are the specific mechanisms in space and time that charge and discharge the equatorial strip? To answer these questions, numerical simulations of the ocean adjustment process to periodic El Niño to La Niña wind stresses were performed. Additionally, a passive tracer was used to help diagnose the mass exchange process that occurs in El Niño - La Niña transitions.

2 The Equatorial β-Plane

The governing equations used to study El Niño are the reduced-gravity shallow-water β-plane equations. The scales of interest in this particular problem are such that the linearized version of these equations is adequate. The familiar equations are

$$\begin{aligned} u_t - v\beta y &= -g' h_x + \mathbb{D}_u + \mathbb{X} \\ v_t + u\beta y &= -g' h_y + \mathbb{D}_v + \mathbb{Y} \\ h_t + H_0(u_x + v_y) &= 0\,. \end{aligned} \tag{1}$$

These equations have been studied extensively and a review can be found in [7]. These particular equations represent a one and a half layer model; a dynamic upper-layer and a denser static lower layer. The reduced gravity, g', is defined as $g' = g(1 - \rho_1/\rho_2)$, and dissipation and forcing are symbolically represented. The appropriate scalings for this set of equations are

$$(x, y) = a_e(\hat{x}, \hat{y})\,, \quad (u, v) = c(\hat{u}, \hat{v})\,, \quad h = H_0\hat{h}\,, \quad \text{and} \quad t = t_0\hat{t} \tag{2}$$

where the length scale a_e is the equatorial Rossby deformation radius, c is the shallow water wave speed, H_0 is the mean thermocline depth around which the equations have been linearized, and t_0 is the time it takes a shallow gravity water wave to cross a deformation radius. For this particular problem we used

$$\begin{aligned} c = \sqrt{g' H_0} &\quad\rightarrow\quad 2.89\,\mathrm{m/s} \\ a_e = \sqrt{c/\beta} &\quad\rightarrow\quad 380\,\mathrm{km} \\ H_0 &\quad\rightarrow\quad 150\,\mathrm{m} \\ t_0 = a_e/c &\quad\rightarrow\quad 1.52\,\mathrm{days}\,, \end{aligned}$$

consistent with the previous models of ENSO. For ENSO, the x scale of interest is much larger than 380 km, and time scales of interest are much larger than 1.52 days. If we instead scale by

$$\begin{aligned}(u,v) &\rightarrow (1, a_e/L_x)\, c && (1, 0.022)c\\ (x,y) &\rightarrow (L_x, a_e) && (17\,\mathrm{Mm}, 380\,\mathrm{km})\\ t &\rightarrow t_0 = L_x/c && (70\,\mathrm{days})\\ h &\rightarrow H_0 && (150\,\mathrm{m})\end{aligned}$$

we arrive at the long-wave equations which are the same as (1) except the terms v_t and $\mathbb{Y}$ both go to zero. Without the *long-wave* approximation, (1) represent equatorially trapped wave modes. To obtain the modes, first (1) is nondimensionalized by (2) to obtain

$$\begin{aligned}u_t - vy &= -h_x + \mathbb{D}_u + \mathbb{X}\\ v_t + uy &= -h_y + \mathbb{D}_v + \mathbb{Y}\\ h_t + u_x + v_y &= 0\end{aligned} \tag{3}$$

where all variables are now nondimensional and the terms representing dissipation and forcing are scaled appropriately. The modes of this system are found by first making the change of variables

$$q = h + u \quad \text{and} \quad r = h - u\,. \tag{4}$$

The equations given by (3) in terms of q, r and v are

$$\begin{aligned}q_t + q_x + v_y - vy &= \mathbb{X}\\ r_t - r_x + v_y + vy &= -\mathbb{X}\\ 2v_t + q_y + qy + r_y - ry &= \mathbb{Y}\,,\end{aligned} \tag{5}$$

where dissipation has been neglected. The normal modes of the unforced non-dissipative equations are found by assuming

$$\begin{pmatrix} q(x,y,t)\\ r(x,y,t)\\ v(x,y,t)\end{pmatrix} = \sum_{n=0}^{\infty} \begin{pmatrix} q(y)\\ r(y)\\ v(y)\end{pmatrix} \exp[i(kx - \sigma t)]\,. \tag{6}$$

The resulting equations are reduced to a single parabolic cylinder equation for v

$$v_{yy} + \left(\sigma^2 - k^2 - \frac{k}{\sigma} - y^2\right) v = 0\,. \tag{7}$$

The physically relevant boundary condition is that $\lim_{|y|\to\infty} |v| = 0$. With this boundary condition σ must satisfy

$$\sigma^2 - k^2 - \frac{k}{\sigma} = 2n + 1\,, \tag{8}$$

where $n \in \{0, 1, \ldots\}$. Additionally, there is a mode for $n = -1$ and it is called the Kelvin mode. This mode is derived from the momentum equations assuming $v = 0$. The mode for $n = 0$ is called the mixed-mode, and there are two modes for $n \geq 1$, inertia-gravity modes (high frequency) and Rossby modes (low frequency). The Kelvin and Rossby modes are

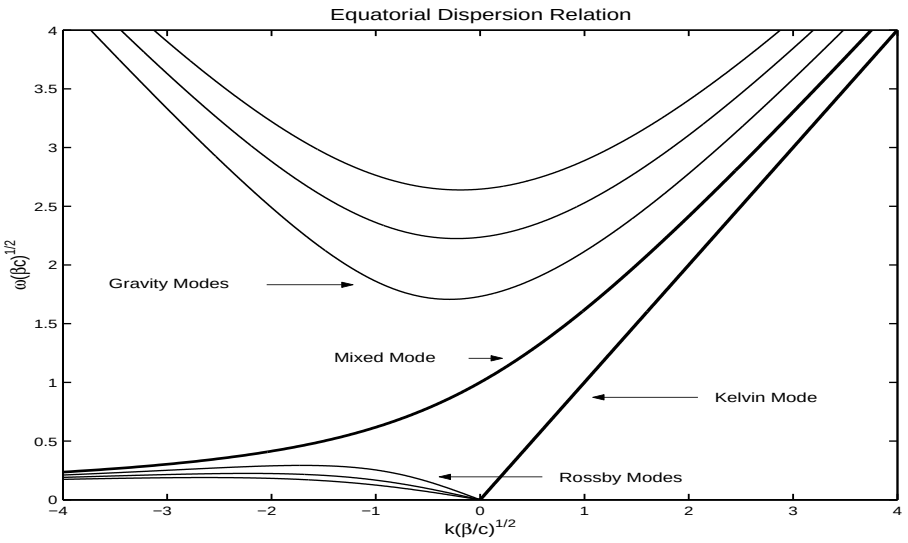

Figure 1: The dispersion relation for equatorial waves. The first three Rossby and gravity wave modes are included. The frequency of Rossby modes decrease with mode number and the frequency of gravity wave modes increase with mode number.

crucial to ENSO as we shall see later. The familiar dispersion relationship is plotted in Fig 1.

The ENSO adjustment process was our primary concern. In order to understand the role of equatorial waves in this adjustment process it is necessary to project the evolution of the system on to the systems modes. Following [2] and subsequently [3], but *not* making the long-wave approximation, we can arrive at amplitude equations for the modes of the system. Instead of assuming oscillatory solutions in x and t, we solve (5) by expanding the y component of these equations in "normalized" parabolic cylinder functions

$$\begin{pmatrix} q(x,y,t) \\ r(x,y,t) \\ v(x,y,t) \end{pmatrix} = \sum_{n=0}^{\infty} \begin{pmatrix} q_n(x,t) \\ r_n(x,t) \\ v_n(x,t) \end{pmatrix} D_n(y)\,, \tag{9}$$

where

$$D_n(y) = \frac{(-1)^n}{\sqrt{2^n n!\sqrt{\pi}}} \exp(y^2/2) \frac{d^n}{dy^n} \exp(-y^2)\,. \tag{10}$$

D_n is considered normalized because

$$\int_{-\infty}^{\infty} D_m D_n \, dy = \delta_{mn}$$

where n is the set of whole numbers. This results in equations for the mode amplitudes

$$\begin{aligned} 2v_{nt} + \sqrt{2(n+1)}q_{n+1} - \sqrt{2n}r_{n-1} &= 2\mathbb{Y}_n \\ q_{nt} + q_{nx} - \sqrt{2n}v_{n-1} &= \mathbb{X}_n \\ r_{nt} - r_{nx} + \sqrt{2(n+1)}v_{n+1} &= -\mathbb{X}_n\,, \end{aligned} \tag{11}$$

with $\mathbb{X}_n$ denoting the x forcing projected on the nth parabolic cylindric function

$$\mathbb{X}_n = \int_{-\infty}^{\infty} \mathbb{X}(y) D_n(y)\, dy\,,$$

similarly for $\mathbb{Y}_n$. This may appear complicated but the evolution equation for the equatorial waves can be found all in terms of q_n, the first two are

$$q_{0t} + q_{0x} = \mathbb{X}_0 \tag{12}$$

$$\sqrt{2} q_{1t} = 2\mathbb{Y}_0 - v_{0t} \tag{13}$$

and for $n \geq 1$

$$(2n+1) q_{(n+1)t} - q_{(n+1)x} = n\mathbb{X}_{n+1} - \sqrt{2(n+1)}\mathbb{X}_{n-1} + \sqrt{2(n+1)}[\frac{\partial}{\partial t} - \frac{\partial}{\partial x}](\mathbb{Y}_n - v_{nt})$$

where

$$v_{nt} = \frac{\partial}{\partial t}(q_{(n+1)t} + q_{(n+1)x} - \mathbb{X}_{n+1})$$

for all $n \geq 0$. The advantage of this notation is that the different wave modes have different y dependence. The amplitude of the Kelvin wave is given by q_0, the mixed wave by q_1, and the Rossby and inertia-gravity waves by q_m, $m \geq 2$. Note that the equation for v_{nt} is displayed separately to emphasize that if the long wave approximation had been made this term would be zero because the terms $v_{nt} = 0$, and $\mathbb{Y}_n = 0$. With this approximation the mixed mode and the gravity modes are not present, hence, the only modes that would survive are the Kelvin (q_0) and the Rossby modes (q_n's). If the long-wave approximation is not made, the Rossby modes and gravity modes have the same y dependence, therefore the modal amplitude $q_2(x,t)$ corresponds to the amplitude of the gravest gravity mode in addition to the the amplitude of the gravest Rossby mode. Thankfully, the scales of interest in this problem are such that the long-wave approximation is certainly valid and the amplitude of q_n with $n \geq 1$ corresponds to the amplitude of the $n \geq 1$ Rossby mode.

3 The Model Setup

The transition between La Niña and El Niño was diagnosed numerically by spinning up the shallow water model to a periodic El Niño to La Niña forcing. Specifically, (1) was solved numerically (see Appendix for details) using a standard shallow water model forced by wind stress fields obtained from a run of the ZCM. These fields can be seen in Figure 2.

The time dependence of the wind stress forcing was given by the function

$$\begin{aligned}\vec{\tau}(t) = &\frac{1}{2}\Big[\vec{\tau}_{El} + \vec{\tau}_{La} + \tanh\big[\alpha(t-1)\big]\big(\vec{\tau}_{El} - \vec{\tau}_{La}\big)\Big] \\ &\times H\big(2 - 4\bmod(t/4)\big) \\ &+ \frac{1}{2}\Big[\vec{\tau}_{EL} + \vec{\tau}_{La} + \tanh\big[\alpha(t-3)\big]\big(\vec{\tau}_{La} - \vec{\tau}_{El}\big)\Big] \\ &\times H\big(4\bmod(t/4) - 2\big)\,,\end{aligned} \tag{14}$$

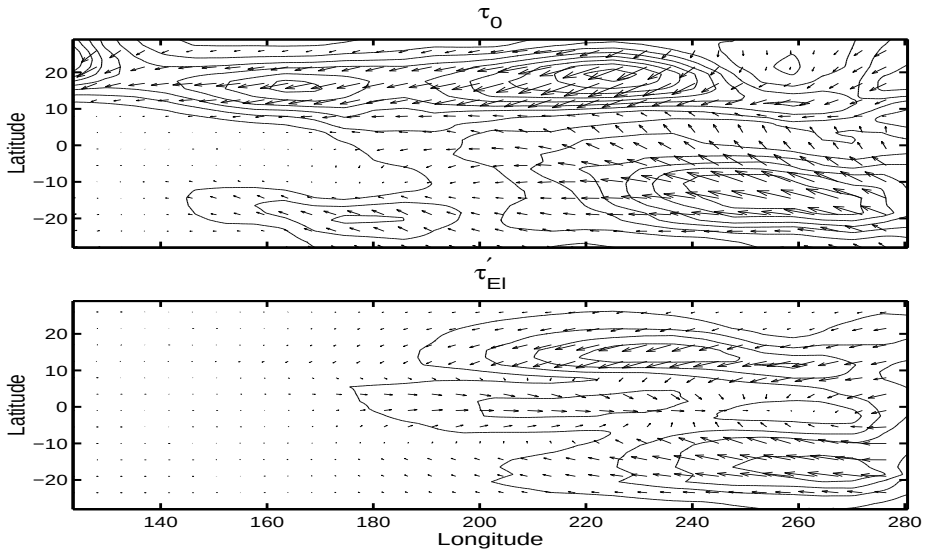

Figure 2: The mean wind stress and the El Niño anomaly. The La Niña anomaly is omitted since it is just the opposite of the El Niño anomaly because the time dependence of the winds is a linear combination of two fields. The total El Niño and La Niña wind stresses are used to force the shallow water model. Contour lines are magnitudes of wind stress in 0.25 dynes/cm^2.

where H is the heavy-side step function and t is measured in years. Figure 3 shows one period (4 years) of the oscillating wind stress. The parameter α is used to adjust how quickly the winds transition from La Niña to El Niño and we set $\alpha = 3$ for all results reported. It is acknowledged that this simple linear interpolation between two wind stress states is a simplification of the true transition process, which includes spatial propagation signals, however, this interpolation is used because it is simple yet physically revealing.

After the model spins up under periodic wind stress forcing, four years of data representing the transition from maximum La Niña winds to maximum El Niño winds and back to La Niña was saved and analyzed. In order to diagnose these idealized La Niña to El Niño

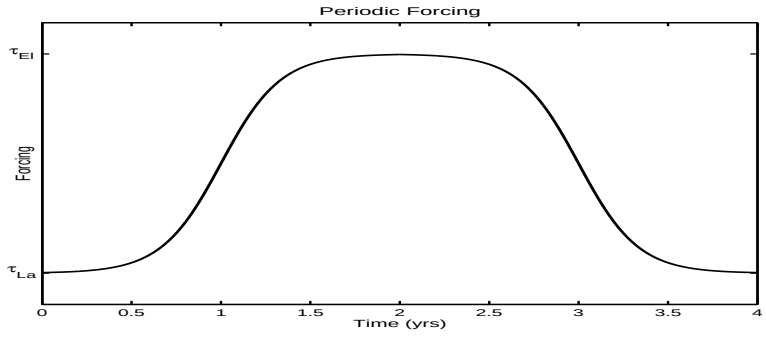

Figure 3: The time dependence of the periodic forcing used in the linear shallow water model used to diagnose the transitions between El Niño and La Niña .

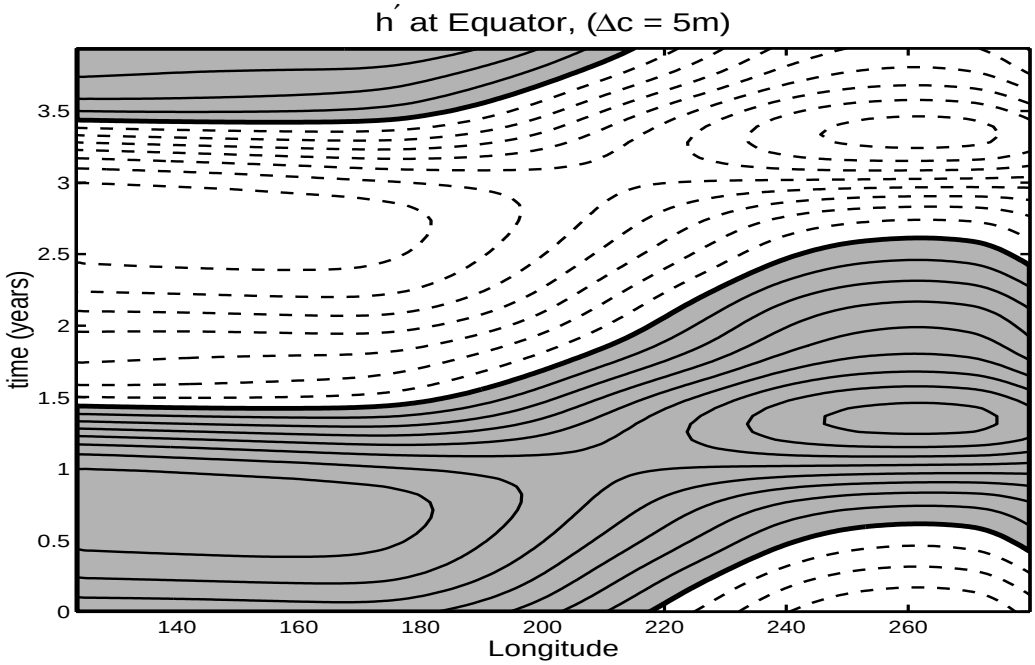

Figure 4: A time-longitude plot of the anomalous height at the equator. The shaded area is positive and the contour level is 5 m.

transitions the fields are split into climatologies and anomalies

$$\begin{aligned} h(x,y,t) &= h_0(x,y) + h'(x,y,t) \\ u(x,y,t) &= u_0(x,y) + u'(x,y,t) \\ v(x,y,t) &= v_0(x,y) + v'(x,y,t)\,. \end{aligned} \tag{15}$$

4 The Role of Waves

The first question to answer is whether these idealized El Niño - La Niña transitions exhibit characteristics implied by the idea of the delayed oscillator. Namely, to what extent are wave dynamics responsible for the time evolution of the anomalous fields? A Hovmöller diagram of h' at the equator is an appropriate place to start, see Figure 4.

From Figure 4 is it possible to see the role of waves in El Niño to La Niña transitions. Between time zero and one we can see a positive depth anomaly encountering the western boundary, this depth anomaly is then reflected and rapidly moves east across the equator between time 0.75 and 1.5. From Figure 4 it is not clear what occurs when this anomaly reaches the eastern boundary at time 1.5. Due to the symmetry of the forcing the negative depth anomaly evolves in the same manner starting at about time 2.5.

However, projecting $q = h' + u'$ on the normal modes of the system can clarify the role of waves in the transition process by explicitly indicating which equatorial waves are excited in the transition process. The evolution of q projected on the Kelvin and first Rossby mode can be seen in Figure 5.

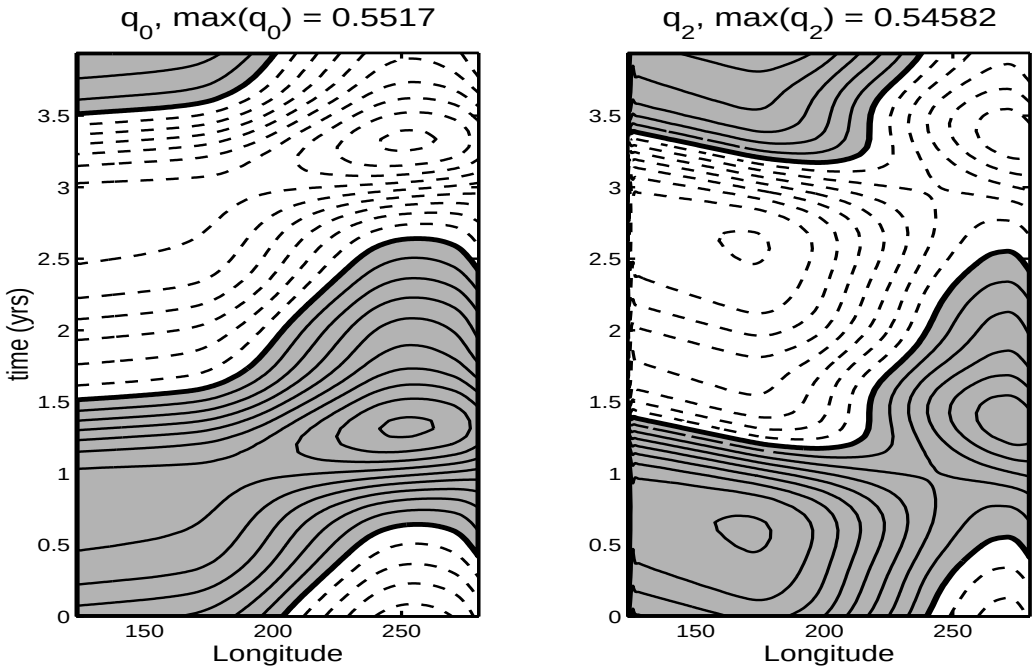

Figure 5: A time-longitude plot of the projection of $q(x, y, t)$ on to the Kelvin mode and the first Rossby mode. The shaded area is positive and the maximum value of the nondimensional projection is displayed.

From Figure 5 the role of the Kelvin and Rossby wave in the transition process is evident. We shall now analyze the positive depth anomaly or warm anomaly in some detail. At $t = 0.5$ the first mode Rossby wave has maximum amplitude near 200° East. This mode propagates along the equator at 1/3 the Kelvin wave speed and then encounters the eastern boundary at $t = .9$.[1] The Rossby wave is then reflected as a Kelvin wave but initially, for $t < 1$, the Kelvin wave loses intensity because the stress anomaly is negative. This is clear from the Kelvin modal amplitude equation (12) where $\mathbb{X}$ is the stress anomaly which is negative at the equator for $-1 < t < 1$. It is negative because during this time there are La Niña winds, hence the Kelvin wave amplitude q_0 decreases. At $t = 1$ the stress anomaly changes sign and the Kelvin wave intensifies. It is this intensification which brings El Niño to its maturity. The idea that an equatorial Rossby wave reflects from the western boundary as a Kelvin wave that is later intensified is the principle of the delayed oscillator. In the delayed oscillator model the equatorial Rossby wave is assumed to be excited by the anomalous wind stress in the central part of the basin from the previous El Niño. Is this the case here? See Figure 6 for the projection of q on the third and fifth Rossby modes. From this figure we see that the projection on the slower equatorial Rossby waves is weaker and occurs at the same time and place, $t = 0$ and x =200° East. We ask, what is responsible for the excitation of these modes?

Figure 7 shows the evolution of $h'(x, y, t)$ through the maximum La Niña wind stress

[1]These times denote the approximate time when the maximum amplitude encounters the eastern boundary, etc.

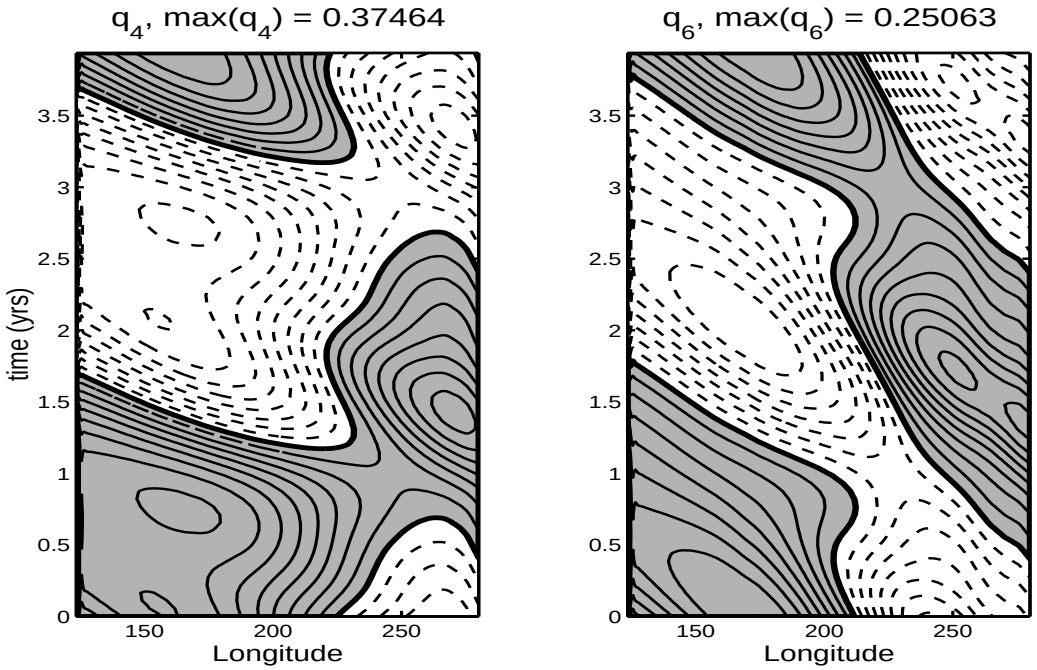

Figure 6: A time-longitude plot of the projection of $q(x, y, t)$ on to the third and fifth Rossby mode. The shaded area is positive and the maximum value of the nondimensional projection is displayed.

anomaly, notice especially the off-equatorial wave near 15° North. It is possible to show that this is a long-QG-Rossby wave at 15° North, i.e. $-a^{-2}\psi_t + \beta\psi_x = 0$, with a speed of about $\beta a^2 \approx 38°/\text{yr}$.

Beginning in panel 2 of Figure 7 this off equatorial long Rossby wave "leaks" into the equatorial region west of 200° E. This is rather unexpected because the delayed oscillator model of El Niño does not address off equatorial dynamics as part of the ENSO mechanism. However, this off equatorial Rossby does eventually "leak" into the equatorial region and excites equatorial Rossby waves that are crucial to ENSO mechanism according to the delayed oscillator mechanism. We will now show that it is the background potential vorticity that allows the off equatorial Rossby wave to leak into the equatorial region. Rossby waves propagate along lines of constant background potential vorticity

$$\zeta = f/H_0\,. \tag{16}$$

Figure 8 shows lines of constant background potential vorticity superimposed on fourth panel of Figure 7.

We see a ridge of high potential vorticity that forces the off equatorial Rossby wave to travel north of 10°. This Rossby wave then "leaks" through the gap in the ridge of potential vorticity at about 170 E Longitude. Again, it is interesting to see off equatorial dynamics playing a role in ENSO transitions, not something usually associated with ENSO, nor is off equatorial dynamics apart of conceptual ENSO models. However, off equatorial dynamics is discussed in the context of El Niño in Philander (1997), where it is discussed in the context of decadal modulations of ENSO variability.

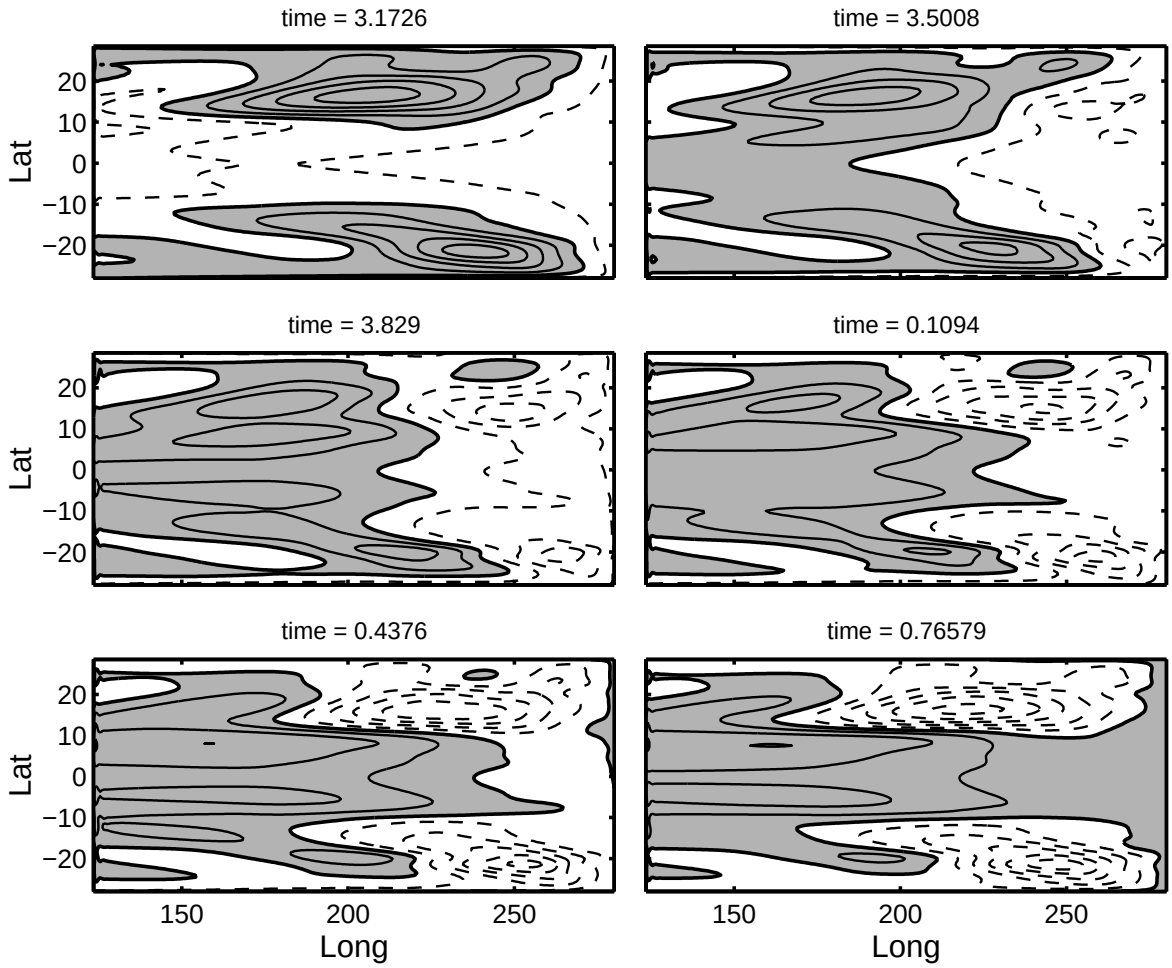

Figure 7: Six frames in the transition through the La Niña wind stress. Maximum La Niña stress anomalies occur at $t = 0$. An off equatorial positive anomaly Rossby wave is clearly seen moving west at around 15° N. Additionally, this Rossby wave can be seen to "leak" into the equatorial region beginning in the second panel. The contour interval is 20 m.

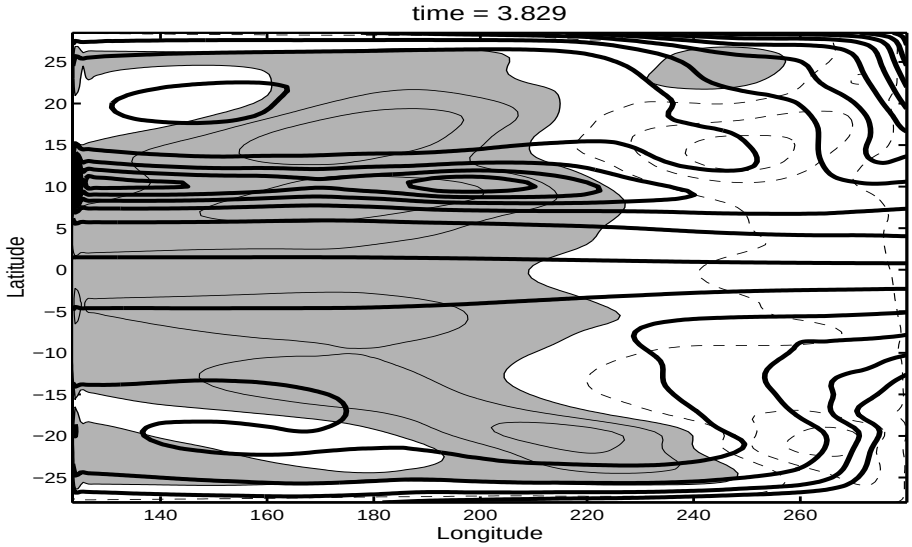

Figure 8: One frame in the transition through the La Niña wind stress with the background potential vorticity contours at a time when the off equatorial Rossby wave is "leaking" into the equator. The contour level for the anomalous height field is 20 m and the potential vorticity field is in bold contours.

5 Recharging and Sverdrup Flow

In the Section 4 it was demonstrated that the wave dynamics view of ENSO is indeed captured in the idealized ENSO transitions we simulated. Can we also see the recharge oscillator perspective in these simulations? If ENSO can be described as a recharge oscillator the total mass (volume) of the equatorial region must oscillate, i.e. the equatorial strip must charge and discharge. According to [5], the recharging takes place prior to an El Niño event, and in the case of our model ENSO transitions this recharging occurs during La Niña wind stresses. Figure 9 shows the zonal mean thermocline depth anomalies and from this Figure we see that the equatorial region has maximum volume prior to the onset of the El Niño, in other words prior to the El Niño wind stress anomaly.

It is obvious from Figure 9 that the equatorial region, between -10° S and 10°, exchanges mass periodically with the off equatorial region, thus these ENSO transitions can be viewed in terms of a recharge oscillator. Can we be more specific about the recharging of the equatorial region? Specifically, what is the mechanism that allows the equatorial region to recharge, and where is the mass responsible for the recharging coming from? It is possible to answer these questions from our idealized El Niño - La Niña transitions. To do so, we will start with the anomalous continuity equation

$$h'_t + H_0(u'_x + v'_y) = -rh' \,. \tag{17}$$

We can now integrate the anomalous continuity equation to obtain the anomalous transport

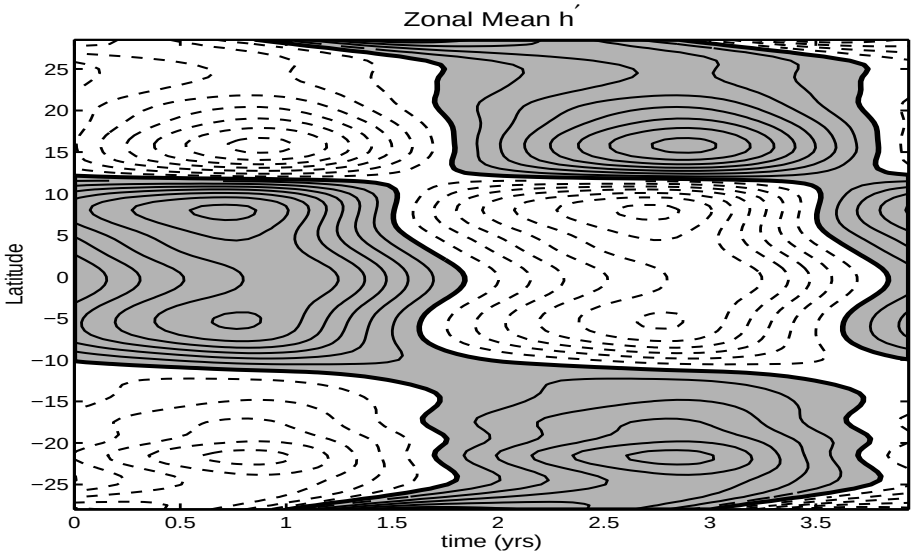

Figure 9: The zonal mean of the thermocline depth anomaly. Notice the recharging and discharging of the equatorial region. The contour interval is 5 m.

into the region east of x,

$$\begin{aligned}\frac{dV}{dt}(x,t) \equiv & \int_{-10^\circ}^{10^\circ}\int_{x}^{X_e} \frac{dh'}{dt}(\tilde{x},y,t)\,dy\,d\tilde{x} = \\ & - r\int_{-10^\circ}^{10^\circ}\int_{x}^{X_e} h'(\tilde{x},y,t)\,dy\,d\tilde{x} \\ & - H_0\int_{x}^{X_e}[v'(\tilde{x},10^\circ,t) - v'(\tilde{x},-10^\circ,t)\,d\tilde{x} \\ & + H_0\int_{-10^\circ}^{10^\circ} u'(x,y,t)\,dy\,.\end{aligned} \tag{18}$$

The total transport into this region, $\frac{dV}{dt}$, has contributions from the relaxation term, $-rh$, meridional velocity at $\pm 10^\circ$, v, and from the zonal velocity u at longitude x. A schematic of this idea is seen in Figure 10. If we let $x = X_w$ in (18) we get the total transport into the equatorial region. This is displayed in Figure 11. This figure clearly shows that the equatorial region is charging during the La Niña phase, $t < 1$ and $t > 3$, and discharging during the El Niño phase, $1 < t < 3$.

From (18) we can deduce where the anomalous transport is taking place such that the equatorial region charges and discharges. Figure 12 is a plot of dV/dt as a function of x for certain times during the recharging phase. This Figure shows where the anomalous velocities, more importantly the anomalous meridional velocities, are transporting anomalous mass into the equatorial region during this phase. In the first panel it is a negative $v'(10^\circ)$ east of 200 E is transporting anomalous mass into the equatorial region. West of 200 E v' is positive but small and is *not* helping to recharge the equatorial region. We can also see that u' is transporting anomalous mass west in the region where v' is transporting anomalous

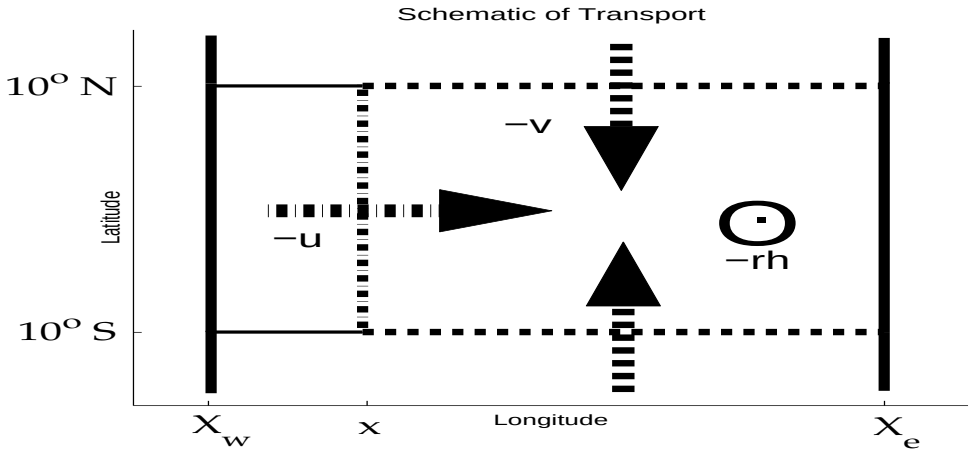

Figure 10: A schematic diagram of the contributions to the transport into the equatorial region east of x.

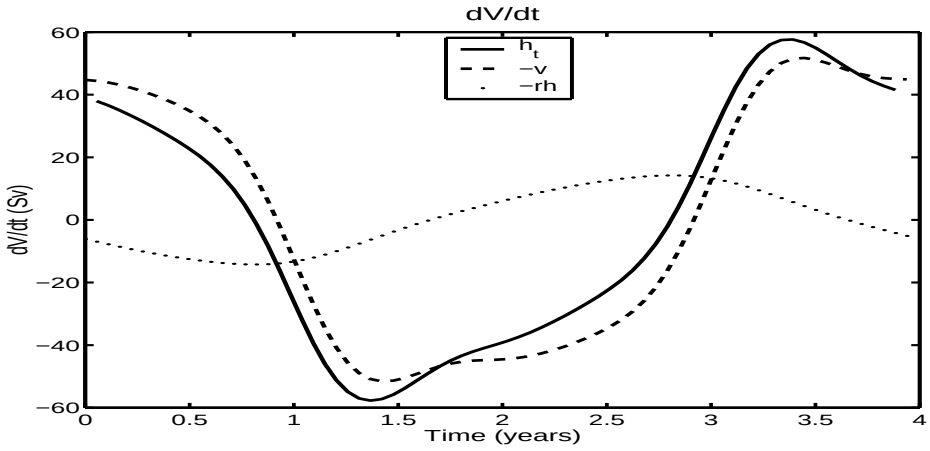

Figure 11: The transport into the entire equatorial region as a function of time. The net transport is depicted by the h_t curve and the contributions to this from the anomalous meridional velocity and the anomalous relaxation are displayed.

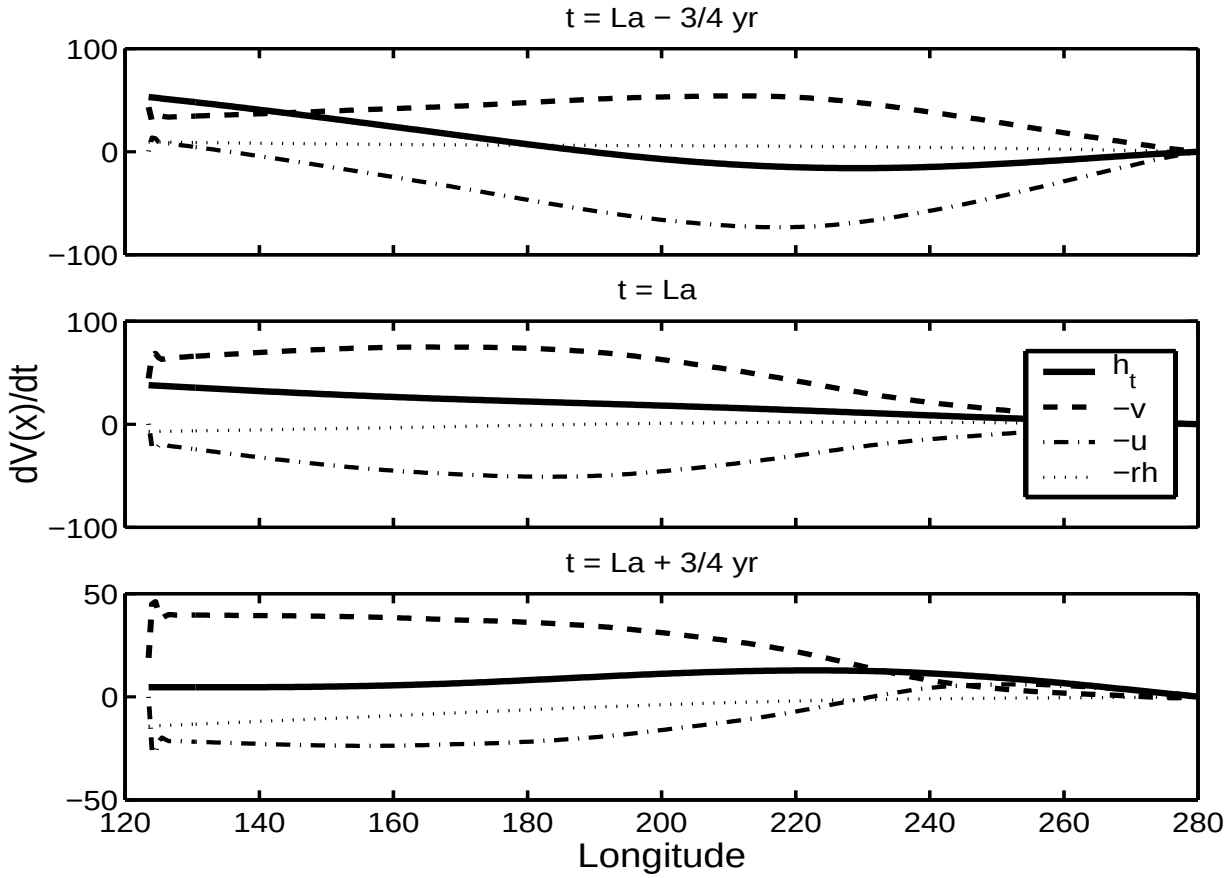

Figure 12: The transport dV/dt into the equatorial region east of x at different times during the recharging phase. The overall transport into the region and the contributions from the anomalous velocities and anomalous relaxation is displayed.

mass into the equator. Note that the anomalous transport due to the boundary current is contributing a small amount to the recharging at this time. In the second panel a negative v' is evident everywhere east of 180 E. This anomalous velocity is responsible for all of the anomalous mass transport into the equatorial region. A negative u' in this same region transports this anomalous mass west. Note that the boundary current is actually helping to expel mass from the equator at this time. Also, the rate at which the equatorial region is filling with mass is approximately constant for all x, i.e. the entire thermocline is filling with water at the same rate. We see this from the constant slope on the h_t curve of this panel. The third panel is at a time close to when the equatorial region begins to discharge. It is possible to see in this panel that the Kelvin wave is helping to transport mass into the eastern equatorial region. Because of the periodic nature of our linear problem and the wind stresses being a linear combination of two states, the discharging process is just the opposite of the charging process.

It was shown that anomalous meridional velocities at $\pm 10^\circ$ mainly in the eastern portion are responsible for the anomalous mass transport that charges and discharges the equatorial

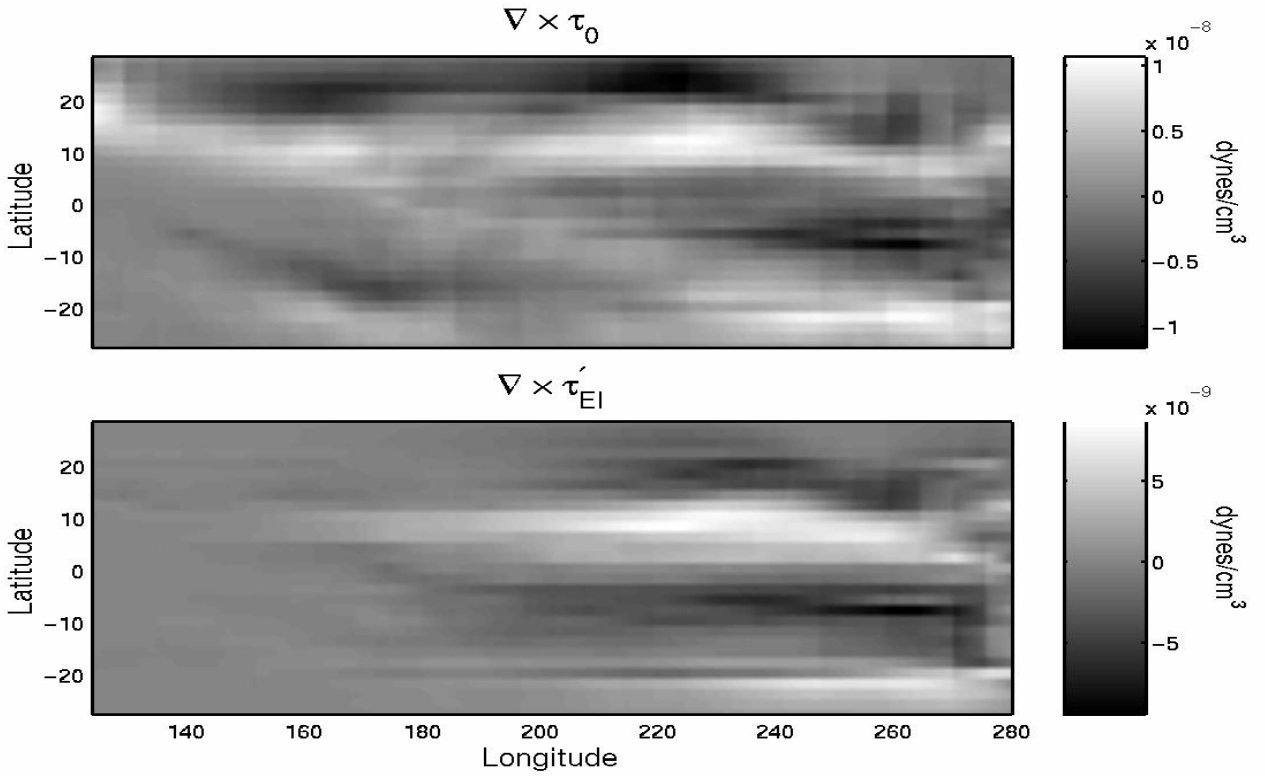

Figure 13: The curl of the mean wind stress field and the curl of the El Niño anomaly wind stress field.

region. From the scales of the problem we would expect the velocities to be in quasi-Sverdrup balance. We can then obtain the anomalous meridional velocities from the anomalous wind stress via the Sverdrup balance

$$\beta v' = \frac{\boldsymbol{\nabla} \times \boldsymbol{\tau}'}{\rho_0 H_0} \cdot \mathbf{k}\,. \tag{19}$$

Figure 13 shows that for El Niño there is a positive wind stress curl anomaly in the eastern equatorial region at 10 N and a negative curl anomaly at 10 S. These anomalous curls are responsible for the discharging of the equatorial region. The curl anomaly for La Niña has the opposite sign as the curl anomaly for El Niño and is hence responsible for the charging of the equatorial region.

Experiments were performed where tracers were injected into the flow at time $t = 0$ with constant gradients in y. These tracers were then advected by the *anomalous* velocities. These experiments were performed to see where the anomalous velocities were present and to show where *anomalous* mass was being transported. These experiments confirmed that anomalous equatorward meridional velocities were indeed responsible for the anomalous mass transport. This anomalous mass enters the eastern equatorial region and is then transported west by anomalous zonal velocities at the equator. Again, because of the symmetrical nature of the forcing the opposite is true for the expulsion of mass during the El Niño phase.

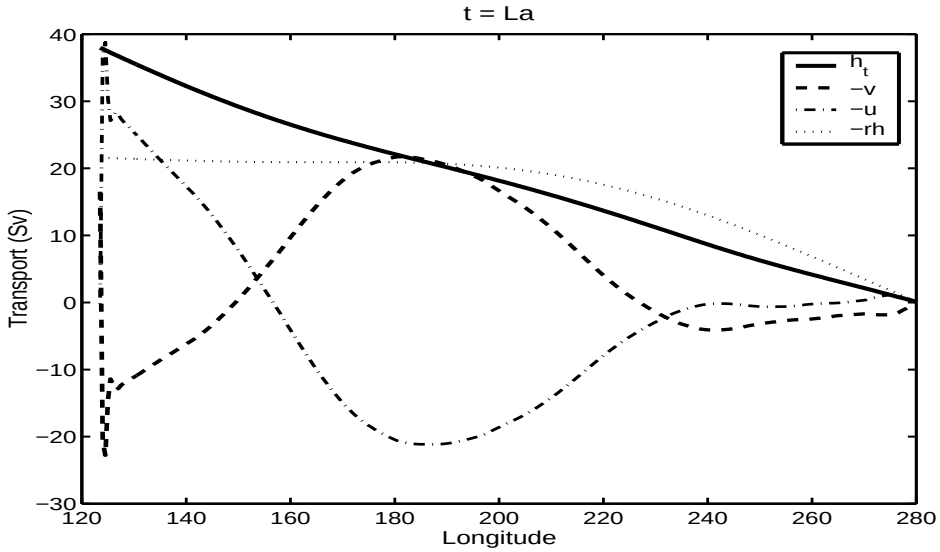

Figure 14: The transport into the equatorial region east of x and the contributions from the full velocity fields and the full relaxation.

6 Total Mass Transport & No Relaxation

The previous sections on transports have emphasized the role of anomalous velocities transporting anomalous mass. In these sections we have isolated what causes the recharging of the equatorial region. However, by using anomalous velocities we do not have a true Lagrangian perspective on the recharging of the equatorial region. In order to determine the origins of the water that actually recharges the equatorial region we must add in the climatological transport to the analysis performed in Section 5. Doing this equation (18) is now an equation that involves the total velocities and Figure 14 displays the total transport into the equatorial region during the recharging phase.

Figure 14 clearly shows that the meridional velocities east of 240 E are transporting mass out of the the equatorial region, between 180 E and 240 E v is transporting mass into the region, and west of 180 E mass is being transported out of the equatorial region. This figure also shows that if it were not for the Western Boundary Current the equatorial region would be losing mass from v transport. We can conclude that it is anomalously weak meridional velocities in the eastern portion of the equatorial region that allows the western boundary current to fill the region. From this figure we see that the relaxation term $(-rh)$ in the continuity equation is actually doing more work than v to recharge the equatorial region. Knowing that this term is a slightly nonphysical parameterization of upwelling and mixing, we should ask whether the recharging of the equatorial region should rely this heavily upon this term? Additionally, is this term necessary for the recharging of the equatorial region?

These questions were answered by running the same experiment but without the relaxation term in the continuity equation. From Figure 15 we see that the equatorial region still charges and discharges, hence the $-rh$ term is not mandatory for the recharging of the equatorial region. Additionally, the the transport analysis was performed on this ex-

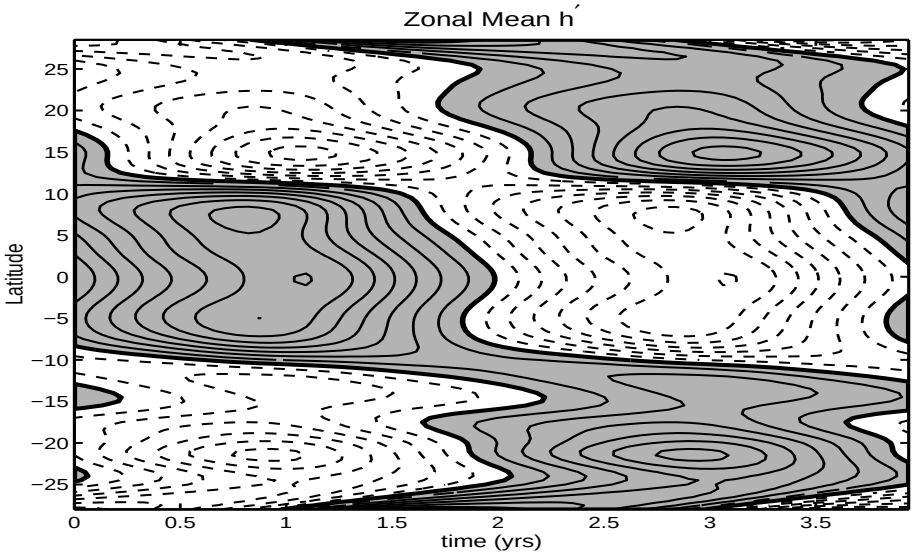

Figure 15: Zonal mean anomalous thermocline depth with no relaxation in the continuity equation.

periment and it was found that in this case the meridional transport is solely responsible for the recharging of the equatorial region. Specifically, it is the weakening of the meridional transport in the out of the basin that allows the western boundary current to fill the equatorial region with anomalous mass, as Figure 16 clearly shows. It is interesting that in Figure the contributions to this charging by u and v are such that the equatorial region is uniformly charging as seen in the constant slope of dh/dt.

7 Conclusions

The purpose of this project was to see if both the wave perspective of ENSO, as exemplified by the delayed oscillator model (Suarex & Schopt 98, Battisti 98), and the mass transport perspective of El Niño , as exemplified by the recharge oscillator model (Jin 97), may be diagnosed in a model simulation of ENSO transitions using a numerical model that is capable of capturing both mechanisms. Both perspectives of ENSO were clearly evident in the idealized ENSO transitions that we modeled. However, as regards to the wave dynamics perspective of ENSO our model shows that it is off equatorial Rossby waves that propagate anomalous thermocline depths from the eastern equatorial region to the west in contrast to equatorially trapped Rossby waves that are emphasized in the delayed oscillator picture of ENSO. The off equatorial Rossby wave does excite equatorial Rossby waves but not until it encounters a gap in the ridge of background potential vorticity in the western portion of the basin where it is able to "leak" into the equatorial region. Thus, this model indicates an interesting interaction between off equatorial dynamics and equatorial dynamics in ENSO transitions (Galanti & Tziperman have also noted this phenomena, personal communication 2001). It is this particular interaction that is worthy of future research.

The mass transport perspective of ENSO was also evident in these idealized ENSO transitions. Using this model we were able to specifically diagnose the mechanisms respon-

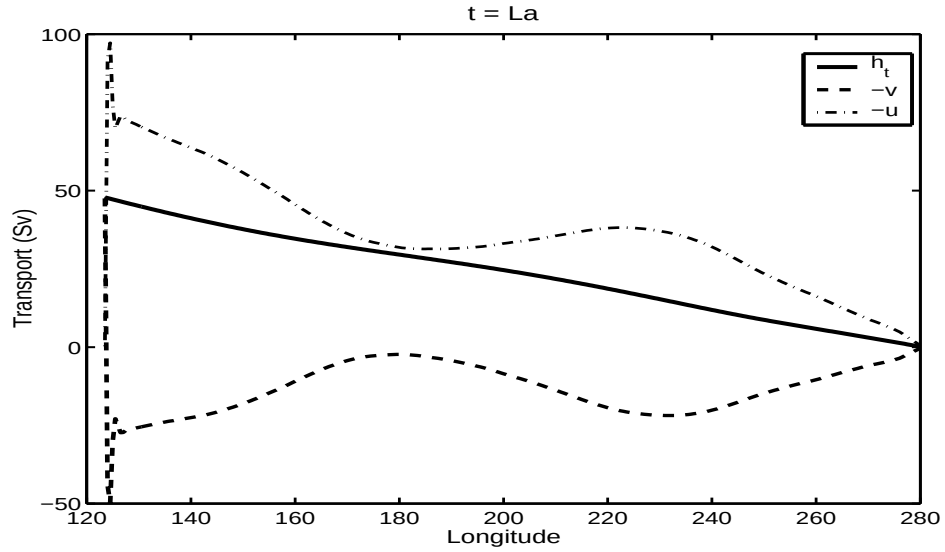

Figure 16: The x dependence of the total transport and the contributions from the full velocity fields with no relaxation in the continuity equation during the recharging phase.

sible for the recharging and discharging of the equatorial region. We found that anomalous wind stress curls in quasi-Sverdrup balance with meridional velocities are responsible for the charging and discharging of the equatorial region. These anomalous wind stress curls are present in the eastern portion of the equatorial region at $\pm 10°$. These anomalous meridional velocities allow the western boundary current to fill the equatorial region with mass. We also found that the $-rh$ term included in most models of ENSO for numerical purposes, is not necessary for the recharging of the equatorial region, nor does it distort the qualitative picture.

8 Thanks

Thanks to the two advisors who helped me with this project, Eli Tziperman for helping me to understand the results herein, and Eric Chassignet for helping to get the results; it was a pleasure working with both of you. Thanks to Paola Cessi for some remarks that forced me to understand and present this work more clearly. Thanks also to the fellows and their support, it was greatly appreciated.

9 Appendix

9.1 Numerical Methods

The numerical model used was a modification of the Bleck and Boudra isopycnic coordinate general circulation model. This code was modified to solve the linear shallow water equations. The model uses a standard "c" grid and a leap frog time stepping scheme. The

model solved the equations

$$\begin{aligned} u_t - v\beta y &= -g' h_x - ru + \nu\nabla^2 u + \frac{\tau^{(x)}}{\rho_0 H_0} \\ v_t + u\beta y &= -g' h_y - rv + \nu\nabla^2 v + \frac{\tau^{(y)}}{\rho_0 H_0} \\ h_t + H_0(u_x + v_y) &= -rh\,. \end{aligned} \tag{20}$$

The resolution of the model was 0.5°, as measured at the equator, in both the x and y directions. The values of most of the constants were given in Section 2. The additional values used were:

$$r = 1/30\,\mathrm{mo}^{-1} \quad \text{and} \quad \nu = 1100\,\mathrm{m}^2\mathrm{s}^{-1}\,. \tag{21}$$

9.2 The Long-wave Approximation

In order to better understand the long wave approximation and why it is relevant to the equatorial basin and ENSO, we examined the reflection of equatorial Kelvin waves by the eastern boundary of a basin. Additionally, this problem was examined to better understand why in the delayed-oscillator model of ENSO eastern boundary reflection is sometimes ignored. The set up is simple, if a Kelvin wave is excited along the equator, perhaps by an anomalous wind stress, it will propagate along the equator until it reaches the eastern boundary of the basin at which point it must be reflected[2]. What is the outcome of this reflection? It can not reflect as a Kelvin wave or a mixed wave; they only propagate energy eastward. It must transmit its energy to coastally-trapped Kelvin waves (or some deviant of a coastally-trapped Kelvin wave[3], equatorially trapped Rossby waves or gravity waves. The structure of the disturbance in k space determines the outcome of this reflection. Consider an initial value problem of the linear shallow water equations. The initial disturbance is

$$\begin{pmatrix} u(x,y,0) \\ v(x,y,0) \\ h(x,y,0) \end{pmatrix} = \begin{pmatrix} \alpha c \\ 0 \\ \alpha H_0 \end{pmatrix} \exp\left(-\frac{\beta}{2c} y^2\right) G(x/L)\,. \tag{22}$$

This initial disturbance is designed to excite an equatorial Kelvin wave response that will propagate to the east with speed c and amplitude α. This disturbance will not disperse because Kelvin waves are not dispersive. We shall choose the specific x dependence to be

$$G(x/L) = \exp[-(x/L)^2]\,. \tag{23}$$

Assuming that the scale of this disturbance is small compared to the size of the basin we can assume that the disturbance is not affected by the presence of the boundaries, and we can analyze this initial disturbance as if x were unbounded. This disturbance excites

[2]Reflected is perhaps not the best word here, the energy fluxed into the eastern boundary of the basin must be fluxed out, and this is what is meant by reflection in this particular usage.

[3]A true coastally-trapped Kelvin wave only exist on an f-plane, therefore true coastally-trapped Kelvin waves can not exist at the equator since f goes to zero there [8].

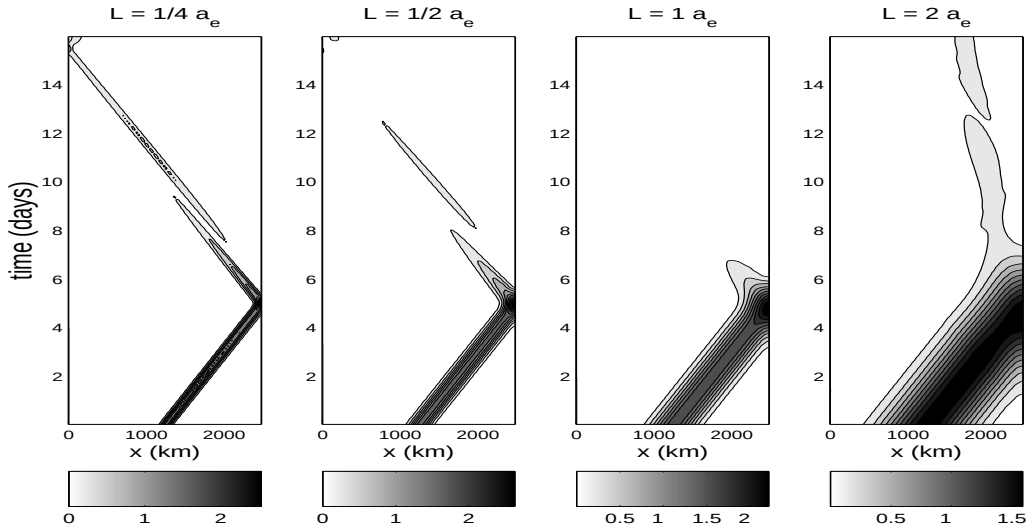

Figure 17: The energy density at the equator, in ergs/cm^2, of an equatorial Kelvin wave as it strikes the eastern boundary of the basin for four different zonal length scales of the disturbance. As the zonal length scale of the disturbance increases, is transmitted to equatorially-trapped gravity waves and more energy is transmitted to equatorial Rossby waves. There are ten equally spaced contours in each panel.

many plane wave Kelvin modes where the amplitude of these excited modes is given by the Fourier transform of (23)

$$\mathcal{G}(k) = \frac{L}{2\sqrt{\pi}} \exp[-(kL/2)^2] \tag{24}$$

assuming that $G(x) = \int_{-\infty}^{\infty} \mathcal{G}(k) \exp(ikx)\, dk$. We see that small initial disturbances (small L) project into high wave number plane waves - obviously the width of Gaussian in k space is inversely proportional to the width of the Gaussian in x space. Since these are Kelvin waves, the frequency is proportional to k ($\omega = ck$) and therefore a small disturbance projects into many high frequency Kelvin modes. When this disturbance encounters the eastern boundary the energy fluxed in must be radiated away by other waves. Some of this energy goes into coastally trapped Kelvin (like) waves that propagate away from the equator and some may be reflected back as either equatorial trapped gravity waves or Rossby waves depending on the frequency of the incident waves. If the disturbance is small, the frequencies may be large enough to reflect as gravity waves. Notice on the dispersion relation, Figure 1, that Kelvin waves with large positive k will have frequencies in the frequency range of the gravity waves.

Typically, simple models of ENSO ignore eastern boundary reflection because the long wave approximation has been assumed and Kelvin waves excited by anomalous wind stresses are assumed to have spatial scales large enough such that these disturbances do not project into high wave number Kelvin modes. When these large disturbances encounter the eastern boundary they will propagate away as coastally trapped Kelvin waves and equatorially trapped Rossby waves. The above analysis showed that Kelvin waves can reflect as fast gravity waves - how large do disturbances need to be such that they will not reflect some of

their energy as gravity waves? For any disturbance the majority of the energy must be in wave numbers less than some critical wave number k_c, where $k_c \sim (3/2)a_e$ according to the dispersion relation. To find the smallest length scale of the disturbance, L, such that the majority of the energy will be in wave numbers less than k_c it is possible to show that the percentage of energy in wave numbers less than k_c, for the Gaussian disturbance (23), is

$$\mathcal{E} = \frac{E(k \le k_c)}{E_0} = \operatorname{erf}\left(\frac{k_c L}{\sqrt{2}}\right) . \tag{25}$$

The percentage of energy in wave numbers less than k_c must be greater than some threshold denoted by $\mathcal{T}$. This results in a bound for L,

$$L \ge \frac{\sqrt{2}}{k_c} \operatorname{erf}^{-1}(\mathcal{T}) . \tag{26}$$

For simplicity let's assume $\mathcal{T} = \operatorname{erf}(1) \approx 0.8427$ so that $L \ge \sqrt{2}/k_c$. As mentioned previously $k_c \sim 3/2a_e$ giving an approximate bound for L,

$$L \ge \frac{2\sqrt{2}}{3} a_e \approx a_e . \tag{27}$$

Thus the zonal length scale of disturbances must be larger than the equatorial deformation radius such that little energy is reflected as gravity waves. This was verified using our shallow water equatorial β-plane model. Four separate cases were considered in which the zonal length scale of the initial disturbance was set to $L = [1/4\ 1/2\ 1\ 2]\, a_e$, respectively. We can clearly see in Figure 17 that as the zonal length scale of the disturbance increases less energy is reflected as equatorially trapped gravity waves. Note that most of the energy fluxed into the boundary leaves as coastally trapped Kelvin waves which can not be seen in Figure 17 because Figure 17 only shows the energy density at the equator. In the fourth panel of Figure 17 notice that some of the incident energy is reflected as an equatorially trapped Rossby wave(s), which is inferred from the speed of this disturbance.

The reflection of the Kelvin wave was also studied by projecting the solution, $u = u(x, y, t)$, $v = v(x, y, t)$, and $h = h(x, y, t)$, on the normal equatorial modes as outlined in Section 2. The projection of the solution on the first five modes of q is given in Figure 18 and Figure 19 for length scales of the disturbance given by $L = [1/4\ 2]\, a_e$, respectively. In these figures the magnitude of the projection is squared and normalized by the magnitude of the Kelvin wave projection. We can see that before the reflection the projection of q is entirely in the equatorial Kelvin mode. For all times the projection of q on to odd numbered modes is very small because the odd numbered modes represent odd structure in y which should not exist because of the symmetric y structure of the initial disturbance. The small projection on these modes is due to numerical inaccuracies. For the small disturbance there is some projection on q_2 after the disturbance has reflected. The speed of this mode is consistent with the speed of the first equatorial gravity wave mode, however this mode is dispersive and the magnitude of the projection can not remain localized in space. Also notice that the maximum magnitude of the projection on this mode is only 6% of the projection on the Kelvin mode. Again this is evidence that most the energy that is in the original Kelvin wave is transferred to coastally trapped Kelvin (like) waves.

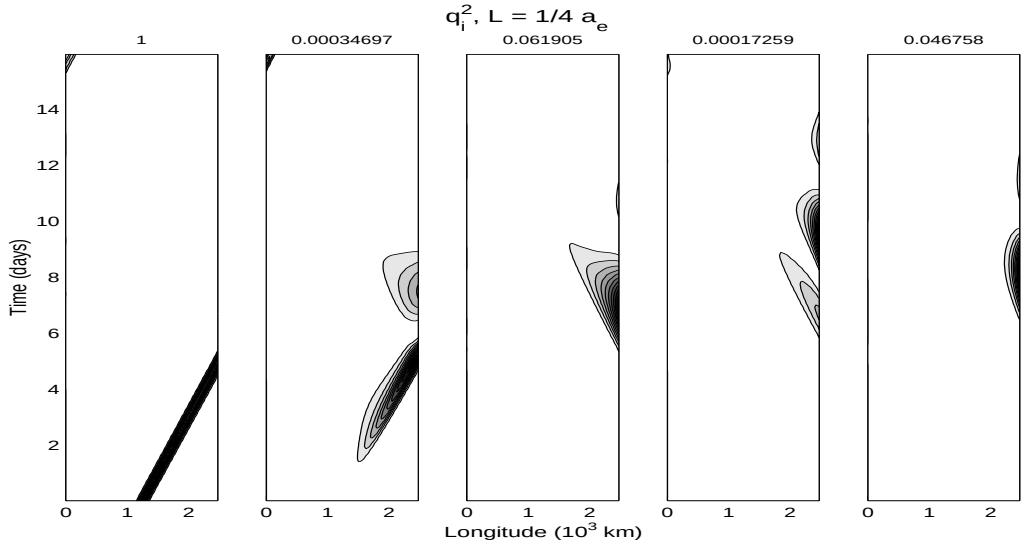

Figure 18: The magnitude squared of the projection of the Kelvin wave disturbance on the first five modes of the equatorial region for an initial disturbance with $L = 1/4\, a_e$. The number at the top of each panel represents $\max(q_i^2)/(\max q_0^2)$. The mode number, i, counts from zero to four, left to right. For all panels there are ten equally spaced contours.

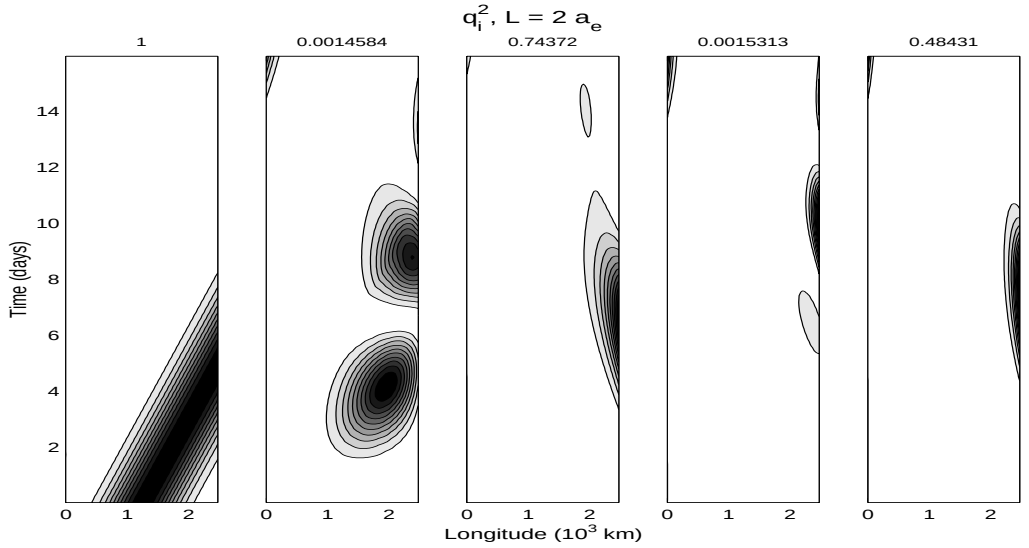

Figure 19: The magnitude squared of the projection of the Kelvin wave disturbance on the first five modes of the equatorial region for an initial disturbance with $L = 2\, a_e$. The number at the top of each panel represents $\max(q_i^2)/\max(q_0^2)$. The mode number counts from zero to four to the right. Notice the strong projection into Rossby mode one as the disturbance encounters the boundary. There are ten equally spaced contours for each panel.

The same procedure was performed with the initial disturbance with a length scale of $L = 2\,a_e$, and the results are in Figure 19. Again we can see that the initial disturbance is a pure equatorial Kelvin mode prior to reflection. However, after reflection the solution projects into the first and third Rossby modes, and these projections have speeds consistent with the appropriate Rossby mode wave speeds. Again the odd numbered modes corresponding to odd y structure are only excited because of numerical inaccuracies.

A discussion of incident waves on the eastern boundary of an equatorial basin is found in [8]. Philander shows that waves of frequency close to $\sqrt{c\beta}$ (the Kelvin and mixed modes) transmit their energy to coastally trapped disturbances of the form

$$v = A\sqrt{y}\exp\left[i\left(\sigma t - \frac{\sigma y}{c} + \frac{\beta x}{2\sigma}\right) - \beta y\frac{L_x - x}{c}\right].$$

We see that eastward-propagating equatorially-trapped waves do not transfer their energy to a coastally-trapped Kelvin waves, but rather a coastally-trapped Kelvin-like wave. Philander also shows that as the frequency of the incident Kelvin wave decreases more energy is reflected as Rossby waves, but there is always a finite amount of energy that is reflected as coastally trapped waves. This is shown by fixing σ in the dispersion relation, (8), and solving for all the possible k's by letting n vary. We find that there is always an infinite number of coastally trapped waves, imaginary k's, for a given σ.

References

[1] S. E. Zebiak and M. A. Cane, "A model el nino-southern oscillation," Mon. Wea. Rev. **115**, 2262 (1987).

[2] A. E. Gill, "Some simple solutions for heat-induced tropical circulation," Quart. J. Roy. Meteorol. Soc. **106**, 447 (1980).

[3] D. S. Battisti, "Dynamics and thermodynamics of a warming event in a coupled tropical atmoshpere-ocean model," jas **45**, 2889 (1988).

[4] M. J. Suarez and P. S. Schopf, "A delayed oscillator for enso," J. Atmos. Sci. **45**, 3283 (1988).

[5] F. Jin, "An equatorial ocean recharge paradigm for enso. part i: Conceptual model," J. Atmos. Sci. **54**, 811 (1997).

[6] F. Jin, "An equatorial recharge paradigm for enso. part ii: A stripped-down coupled model," J. Atmos. Sci. **54**, 830 (1997).

[7] A. E. Gill, *Atmoshpere-Ocean Dynamics* (Academic Press, San Diego, 1982).

[8] S. G. Philander, *El Nino, La Nina, and the Southern Oscillation* (Academic Press, San Diego, 1990).